Photochemistry of Protonated Nitrosamine: Chemical Inertia of NH_2NOH^+ Versus Reactivity of NH_3NO^+

Daniel Peláez, Juan F. Arenas, Juan C. Otero, Francisco J. Ávila, and Juan Soto*

Department of Physical Chemistry, Faculty of Sciences, University of Málaga, E-29071 Málaga, Spain

Received: April 15, 2008; Revised Manuscript Received: June 13, 2008

The photochemical behavior of the protonated simplest nitrosamine $[NH_2NO-H]^+$ has been addressed by means of the CASPT2//CASSCF methodology in conjunction with the ANO-L basis sets. The relative stability of the different tautomers, namely, (1) NH_2NOH^+, (2) NH_3NO^+, and (3) NH_2NHO^+, has been considered, and the corresponding tautomerization transition states have been characterized. With respect to the most chemically relevant species, it has been found that NH_2NOH^+ corresponds to a bound structure, while NH_3NO^+ corresponds to an adduct between NH_3 and NO^+ at both CASSCF and CASPT2 levels of theory. Vertical transition calculations and linear interpolations on the homolytic dissociation of NH_3NO^+ in combination with previous results on neutral nitrosamine [*J. Chem. Phys.* **2006**, *125*, 164311] and neutral *N*,*N*-dimethylnitrosamine [*J. Org. Chem.* **2007**, *72*, 4741] indicate that, in acidic diluted solutions, the protonation of nitrosamine takes place on the excited surface. The N−N dissociation channels have been studied both in ground and first excited singlet state. An S_1/S_0 conical intersection is found to be responsible for the photostability of NH_2NOH^+. On the contrary, NH_3NO^+ is photochemically unstable as its first excited state is purely dissociative. The latter species is characterized by a twofold reactivity: the formation of nitrosyl cation (NO^+) in the ground state and the photorelease of physiologically relevant nitric oxide radical (NO) in its first excited state.

Introduction

Since the initial report on the carcinogenic character of simple nitrosamines,[1] great attention has been paid to this family of substances,[2] and major efforts have been devoted to their detection and removal.[3−6] In this respect, photolysis has yielded promising results.[5]

The chemistry of nitrosamines can be divided in two: (1) gas phase chemistry and (2) solution chemistry. With respect to the former, we have recently described the photochemical decomposition of the simplest nitrosamines, namely, parent nitrosamine (NH_2NO)[7] and *N*-nitrosodimethylamine ($(CH_3)_2NNO$),[8] after excitation to the S_1 and S_2 states. The proposed mechanisms, fully coincident in both systems, are also in agreement with experiment[9] and with previous theoretical works.[10] Hence, this can be considered as the prototypical behavior for the photolysis of simple aliphatic nitrosamines.

On the other hand, the chemistry of alkyl nitrosamines in solution is characterized by the occurrence of the aminium radicals (NR_3^+) as early recognized by several authors.[11−13] In the presence of a dilute acid, nitrosamines rapidly photodissociate into aminium radicals (NR_3^+) and nitric oxide (NO). On the contrary, at high concentration of acid, nitrosamines become protonated and do not undergo photolysis. In this respect, protonated nitrosamine has been proposed as an intermediate in the environmentally relevant removal of nitrogen oxides, that is, the DeNOx process,[14] with both experimental[15] and theoretical work[16] supporting this hypothesis. Regarding the low acid concentration case, an association between nitrosamine and the acid has been demonstrated to occur. According to the study of Layne et al.,[17] such association involves the oxygen atom of nitrosamine. Furthermore, Chow et al. analyzed the role played by the associated acid.[18] For such purpose, these authors performed low-temperature irradiation experiments in an anhydrous solid matrix in the presence of CF_3CO_2H. Their results can be summarized as follows: (1) a nitrosamine−acid complex is observed; (2) upon irradiation, a structured UV absorption spectrum with bands at 367, 343, and 333 nm is obtained; (3) when irradiated at 313 nm, a second species is formed, as indicated by its UV spectrum with peaks at lower frequencies, 391, 375, and 362 nm; (4) this new species reverts to the original one upon warming, and (5) at room temperature, a similar solution photolyzes at 313 nm yielding the corresponding aminium radicals. This is summarized in Scheme 1.

SCHEME 1: Chemical Reactivity of Dimethyl Nitrosamine in Diluted Acidic Conditions[a]

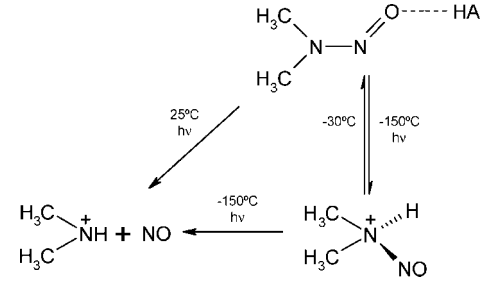

[a] As suggested by Chow et al.,[18] HA denotes the acid molecule.

From the biological point of view, it is remarkable that recent studies have highlighted the physiological role of nitrosamines as sources of nitric oxide radical (NO)[19,20] which constitutes the simplest intra- and intercellular signaling molecule.[21] In this respect, Ohwada et al. have analyzed the structural factors in relation to the NO donor character in a series of nitrosamines. According to their findings, the NO release was favored in those

* To whom correspondence should be addressed. E-mail: soto@uma.es.

10.1021/jp803252h CCC: $40.75
Published on Web 08/19/2008

SCHEME 2: Ground State Relevant Conformations of Protonated Nitrosamine

(a) *trans*-NH_2NOH^+ (b) *cis*-NH_2NOH^- (c) *cis*-NH_3NO^+ (d) NH_2NHO^+

molecules possessing a small N−NO rotational barrier, a factor which is directly linked to the delocalization of the lone pair of the amino nitrogen to the N−O bond. Hence, they concluded that aliphatic nitrosamines do not constitute efficient sources of NO.[20]

In this work, we address the study of the photochemistry of protonated aliphatic nitrosamines by means of the model protonated nitrosamine. The obtained results aim to provide a deeper insight in the chemistry of nitrosamines in solution and, particularly, in their NO donor character. It must be stressed that there has not been any previous report on their photochemistry despite the highly desirable property of finding NO-donating compounds with well-controlled release for medicinal purposes.[20]

This article is structured as follows. Section 2 introduces the methods of calculation. In Section 3, we analyze the chemistry in the ground state focusing on the relative stability of the different conformers, the transition states connecting them, and the relevant N−N bond dissociation channels and, second, we study the chemistry in the upper surface stressing the role played by the surface crossings (conical intersections) and the energetically allowed channels. Section 4 summarizes the main results and concludes the paper.

Computational Details

In this work, we have made use of the CASPT2//CASSCF[22,23] methodology in conjunction with the ANO-L basis set[24] with the C, N, O [4s3p2d1f]/H [3s2p1d] contraction scheme as implemented in the MOLCAS 6.4 set of programs.[25] The location of the conical intersections, that is, same-multiplicity surface crossings, has been performed with GAUSSIAN 03.[26] This protocol has been extensively proven to yield accurate and reliable results on the chemical behavior of related systems.[7,8,28−32] Molecular conformations, normal modes associated with imagi-

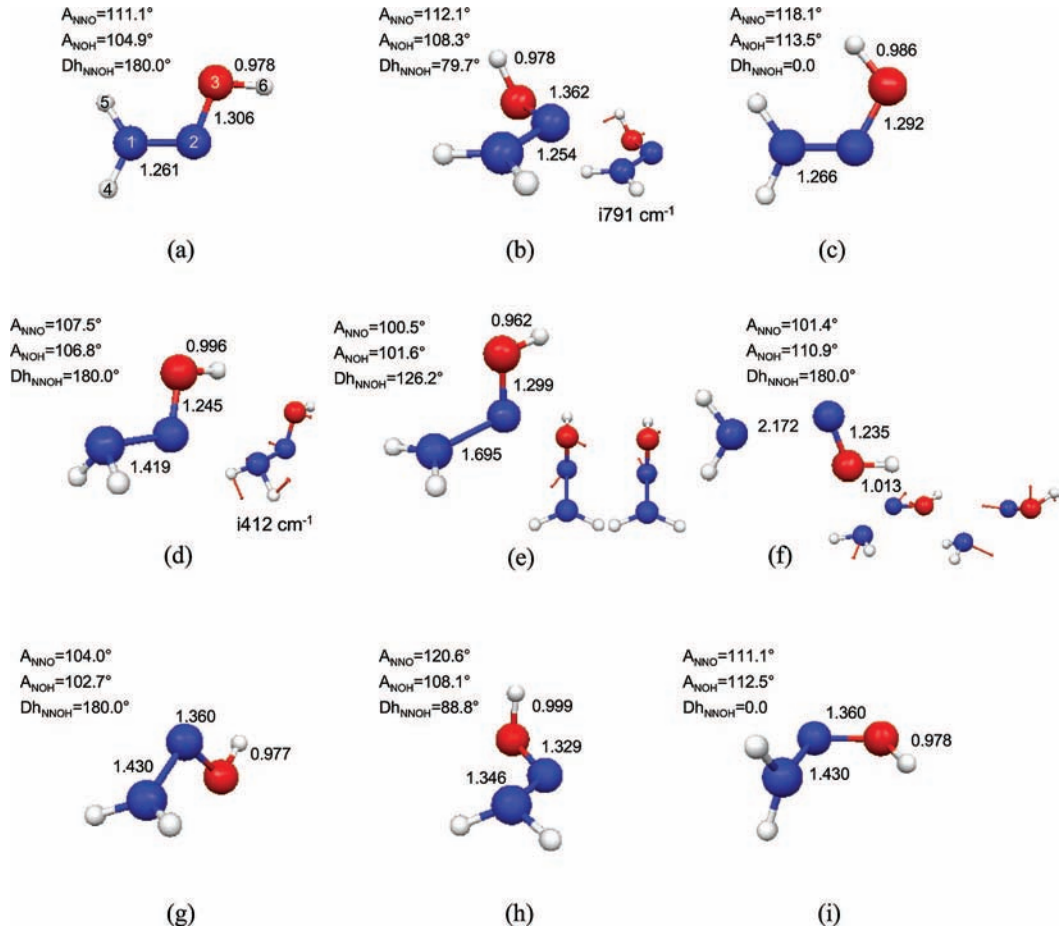

Figure 1. CASSCF critical points of NH_2NOH^+ related to its chemistry on the ground state and the first excited state: (a) *trans*-NH_2NOH^+ minimum (S_0); (b) cis−trans isomerization first-order saddle point; (c) *cis*-NH_2NOH^+ minimum (S_0); (d) NH_2 rotation first-order saddle point (S_0); (e) S_1/S_0 conical intersection; (f) S_1/S_0 conical intersection; (g) NH_2NOH^+ staggered minimum (S_1); (h) NH_2NOH^+ twisted minimum (S_1); and (i) *cis*-NH_2NOH^+ minimum (S_1). Smaller structures correspond to (1) imaginary modes on the saddle points and (2) gradient difference and nonadiabatic derivative coupling vectors on the conical intersections. Angle labels are defined according to connectivity.

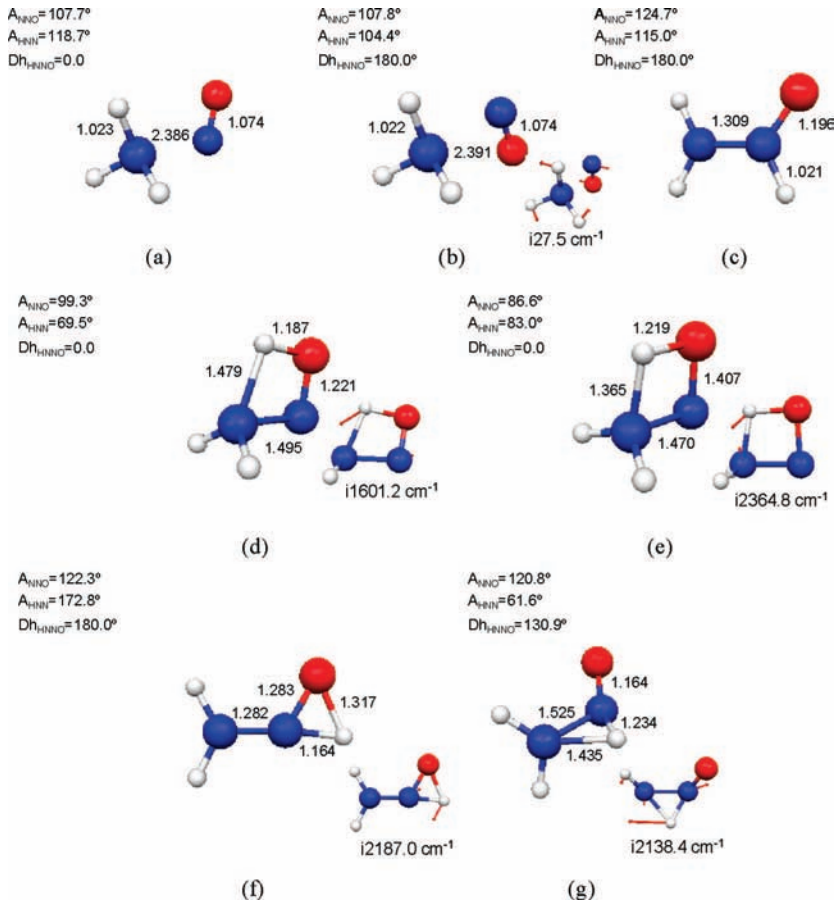

Figure 2. Relevant CASSCF critical points of the NH_2NOH^+ tautomers and relevant transition states corresponding to their interconversions: (a) *cis*-NH_3NO^+ minimum (S_0); (b) *trans*-NH_3NO^+ first-order saddle point; (c) NH_2NHO^+ minimum (S_0); (d) transition state for the $NH_2NOH^+ \rightarrow NH_3NO^+$ interconversion in S_0; (e) transition state for the $NH_2NOH^+ \rightarrow NH_3NO^+$ interconversion in S_1; (f) transition state for the $NH_2NOH^+ \rightarrow NH_2NHO^+$ interconversion in S_0; (g) transition state for the $NH_2NHO^+ \rightarrow NH_3NO^+$ in S_0. Smaller structures correspond to the modes associated with imaginary frequencies. By convention, the angles are defined to start at the migrating hydrogen followed by the closest nitrogen atom.

nary frequencies, and nonadiabatic coupling (NAC) and gradient difference (GD) vectors have been plotted with the MacMolPlt software.[33]

All of the stationary points have been optimized at the CASSCF level of calculation. Moreover, the most relevant structures in ground-state structures have been optimized at the CASPT2 level (see Table 1). Minima and saddle points have been characterized by means of their harmonic vibrational CASSCF/ANO-L frequencies. Additionally, the imaginary modes associated with Franck−Condon geometries have been studied by computation of the CASSCF/ANO-L harmonic vibrational frequencies obtained from the mass-weighted Cartesian forces matrix, that is, Hessian matrix, after projecting out the contributions of the gradients, rotations, and translations as described in a previous work.[34] The nature of the transition states has been verified by computing the corresponding intrinsic reaction paths. This technique has been also applied to those cases where the starting point is nonstationary, for example, Franck−Condon geometry or a conical intersection. In these cases, the initial directions correspond to the associated imaginary modes of the Franck−Condon points and the gradient difference and the nonadiabatic coupling vectors for the conical intersections. In both cases, the general term of minimum energy path (MEP) will be used.

The active space, which has been chosen according to that of neutral nitrosamine,[7] comprises 14 electrons distributed among 11 valence orbitals:

$2s_O$, $2s_N$, σ_{XH}, σ_{NN}, π_{NO}, σ_{NO}, np_N, π_{NO}^*, σ_{NN}^*, σ_{NO}^*, σ_{XH}^* where X = N or O depending on the tautomer. The CASPT2 calculations have been computed over a CASSCF reference wave function by leaving the core orbitals ($1s_C$, $1s_N$, $1s_O$) frozen, that is, as optimized at the CASSCF level.

On the other hand, the geometries of the relevant dissociation fragments have been computed at the following levels of theory: (1) NH_3 (1^1A_1), CASSCF(2,1)/ANO-L [d_{NH} = 0.988 Å, A_{HNH} = 112.0°]; (2) NH_3^+ ($1^2A_2''$), CASSCF(3,2)/ANO-L [d_{NH} = 1.008 Å, A_{HNH} = 120.0°]; (3) NO^+ ($X^1\Sigma^+$), CASSCF(10,8)/ANO-L, [d_{NO} = 1.068 Å]; (4) NOH^+ ($1^2A'$), CASSCF(1,1) [d_{NO} = 1.150 Å, d_{OH} = 0.987 Å, A_{NOH} = 116.8°]. The parameters of NO ($X^2\Pi$) [d_{NO} = 1.157 Å] and NH_2 (1^2B_1) [d_{NH} = 1.008 Å, A_{HNH} = 104.6°] have been obtained from a previous work.[7]

The relevant chemical paths have been studied by means of linear interpolations in internal coordinates. These linear interpolations are obtained as follows: electronic energies are represented versus an interpolation vector, $\Delta\mathbf{R}$, which connects ground states of stable molecules with their respective products. This vector is built by calculating the difference between internal coordinates of reactant and products, $\Delta\mathbf{R} = \mathbf{R}_i - \mathbf{R}_j$, where $\mathbf{R}_i$ and $\mathbf{R}_j$ represent the internal coordinate vectors of the initial and final point, respectively.[30] To minimize the contamination of the perturbed wave function by intruder states as well as to ensure an acceptable weight of the CASSCF reference wave function, the technique of imaginary level shift[35] has been introduced as default in all of the linear interpolation calcula-

TABLE 1: Comparison between Selected CASSCF and CASPT2 Parameters for the Relevant Ground-State Stationary Geometries[a,b]

	t-NH_2NOH^+		*c*-NH_2NOH^+		*c*-NH_3NO^+		*t*-NH_3NO^+		*t*-NH_2NOH^+	
param.[c]	CAS	PT2	CAS	PT2	CAS	PT2	CAS	PT2	CAS	PT2
d_{21}	1.261	1.255	1.266	1.261	2.386	1.951	2.391	1.954	1.309	1.300
d_{32}	1.306	1.306	1.292	1.291	1.074	1.114	1.074	1.114	1.196	1.198
d_{41}	1.007	1.023	1.006	1.023	1.003	1.017	1.003	1.017	1.001	1.016
d_{51}	1.002	1.015	1.003	1.017	1.003	1.017	1.003	1.017	0.998	1.013
d_{63}	0.978	0.976	0.986	0.985	3.207	2.747	3.591	3.320	1.925	1.948
A_{321}	111.1	110.5	118.1	117.8	107.7	111.7	107.8	111.5	124.7	124.8
A_{412}	122.0	122.1	124.5	124.9	109.4	106.5	116.4	109.7	117.4	117.4
A_{512}	115.7	115.8	114.7	114.9	109.4	106.5	116.4	109.7	118.3	118.8
A_{632}	104.9	105.7	113.5	114.5	70.0	66.5	38.1	31.0	27.3	27.4
Dh_{4123}	0.0	0.0	0.0	0.0	−121.8	−121.3	63.6	60.8	0.0	0.0
Dh_{5123}	180.0	180.0	180.0	180.0	121.8	121.3	−63.6	−60.8	180.0	180.0
Dh_{6321}	180.0	180.0	0.0	0.0	0.0	0.0	0.0	0.0	180.0	180.0

[a] Labels *t*- and *c*- denote *trans*- and *cis*-, respectively. [b] Level of theory CAS denotes CASSCF(14,11) wave function, and PT2 denotes CASPT1 wave function with a CASSCF(14,11) reference function. [c] Selected parameters where d_{xy} stands for internuclear distance between atoms (x, y), A_{xyz} stands for valence angle among atoms (x, y, z), and Dh_{xyzw} stands for dihedral angle among atoms (x, y, z, w). Numbering is according to Figure 1a. In all cases, the migrating H corresponds to number 6.

tions. By doing this, we prevent situations in which the weight of the CASSCF wave function in the perturbative treatment results is too low, and as a consequence, the CASPT2 potential energy surface is not continuous. In such cases, the CASPT2 treatment would lack significance.

The transition dipole moments were computed according to the CAS state interaction (CASSI) procedure[36] in conjunction with the perturbatively modified CAS (PMCAS-CI) reference functions obtained as linear combinations of all the states involved in the MS-CASPT2 calculation.

Results and Discussion

This section is structured in four parts. First, the ground state is addressed in terms of energies and character of the relevant stationary points, minima, and transition states for the tautomerizations. Second, the N−N homolytic dissociation is considered for the main conformers, NH_2NOH^+ and NH_3NO^+, and in particular their adiabatic dissociation products are analyzed. In the third part, we discuss the nature of the absorbing species by means of vertical transition calculations. In the final subsection, we compare the photochemical inertia of NH_2NOH^+ in contrast to the photolability of NH_3NO^+ which, in turn, is directly related to the photorelease of nitric oxide. Because experimental works have dealt exclusively with the first excited singlet state,[11−13,18] our discussion will also be focused on such a state.

A. Relative Stability of Tautomers in the Ground State. Protonated nitrosamine exhibits four stable conformers at the CASPT2 and CASSCF levels of theory. These correspond to four minima, namely, (1) *trans*-NH_2NOH^+, (2) *cis*-NH_2NOH^+, (3) *cis*-NH_3NO^+, and (4) NH_2NHO^+ as presented in Scheme 2.

By means of a Mulliken population analysis in neutral nitrosamine, it can be established that two main protonation sites are available: the amino group with a charge of −0.42 e on the N atom and the nitroso group with a charge of −0.31 e in the O atom. A third site corresponding to the N atom of the nitroso group exhibits a low density of charge (−0.01 e), and hence protonation at this point is not favored. The relevant geometries related to the photochemistry of protonated nitrosamine are presented in Figures 1 and 2.

A major difference is observed between the O-protonated (Figure 1a) and the amino-protonated tautomer (Figure 2a) at both CASSCF and CASPT2 levels of theory. While the former corresponds to a covalent bound molecule, the latter corresponds to a weakly bound system, that is, an adduct between nitrosyl cation (NO^+) and ammonia (NH_3), in agreement with previous works.[37,38] For such a structure, our calculations predict a partial positive charge in the NO fragment, +0.897 (+0.569) au at the CASSCF (CASPT2) level of calculation. Furthermore, its N−N bond scission products in the ground state are NH_3 and NO^+ (vide infra). The N−N distance is 2.386 Å and the N−O distance is 1.074 Å at the CASSCF level. The CASPT2 description, although qualitatively similar, predicts a smaller N−N distance of 1.951 Å. By comparing the large shift in the internuclear distance between the CASSCF and the CASPT2 geometries (0.435 Å) and the relatively small CASPT2 energy difference between both structures ($\Delta E \sim 6$ kcal/mol), it is concluded that the adduct corresponds to a shallow minimum. This is further confirmed by the somewhat low values of the N−N bond stretching frequency (CASSCF) which is computed at ∼202 cm^{-1} compared to the corresponding value in neutral nitrosamine which occurs at ∼1005 cm^{-1}.[7] The *trans*-NH_3NO^+ could also be optimized at both levels and corresponds to a CASSCF first-order saddle point. Hereafter, unless otherwise stated, NH_3NO^+ will refer to *cis*-NH_3NO^+. Table 1 collects the CASSCF and CASPT2 sets of parameters for the relevant ground-state stationary points.

The transition states for the tautomerizations in the ground state, namely, (a) *cis*-$NH_2NOH^+ \rightarrow NH_3NO^+$ ($\Delta E = 59.2$ kcal/mol) (Figure 2d), (b) *trans*-$NH_2NOH^+ \rightarrow NH_2NHO^+$ ($\Delta E = 63.2$ kcal/mol) (Figure 2f), and (c) $NH_3NO^+ \rightarrow NH_2NHO^+$ ($\Delta E = 75.8$ kcal/mol) (Figure 2g), have been located. All of the previous energies are referred to *trans*-NH_2NOH^+. As it can be seen, the first one corresponds to a four-center structure (Figure 2d) while the others (Figure 2f and g) correspond to three-center geometries. These points have been further characterized by means of MEP calculations (Figure 3). Table 2 collects the relative energies of the relevant conformers and tautomers of protonated nitrosamines.

B. N−N Homolytic Bond Scissions. The N−N dissociation paths for the most stable and relevant tautomers, that is, *trans*-NH_2NOH^+ and *cis*-NH_3NO^+, have been studied by means of linear interpolations in internal coordinates. The lowest asymptotic channel yields amidogen radical (NH_2) and isonitroxyl cation (NOH^+) in the former and ammonia (NH_3) and nitrosyl

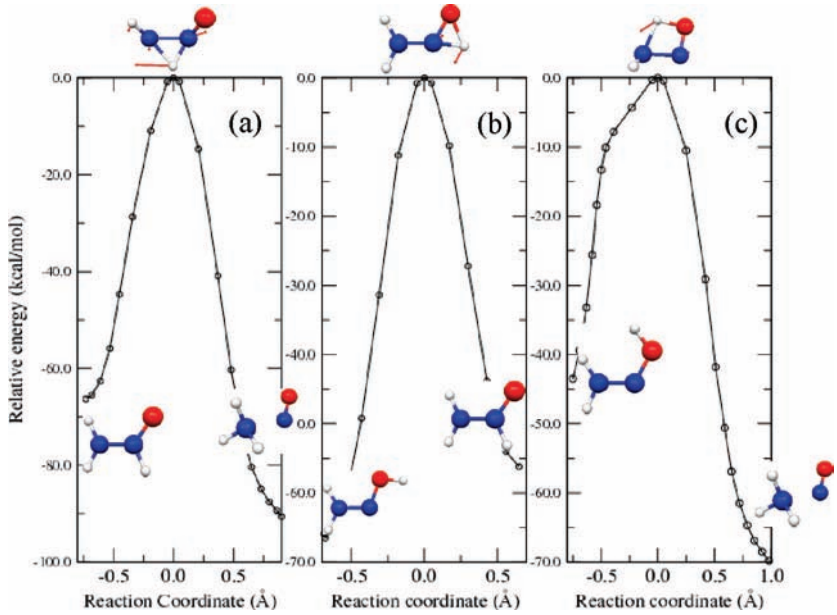

Figure 3. CASSCF minimum energy paths corresponding to the tautomerizations between (a) NH_2NHO^+ and NH_3NO^+; (b) *trans*-NH_2NOH^+ and NH_2NHO^+; and (c) *cis*-NH_2NOH^+ and NH_3NO^+. Energies are referred to that of the corresponding transition state (structure represented on the top of the curves).

TABLE 2: Energies of the Photochemically Relevant Points of Protonated Nitrosamine on the Ground and First Singlet Excited States

geometry[a]	configuration[b]	w^c	ΔE^d	ref[e]	CASSCF[f]	CASPT2[g]
Figure 1a, S_0	G.S.	0.92	0.0	0.90	−0.39791	−0.86740
Figure 1c, S_0	G.S.	0.92	11.3	0.90	−0.38040	−0.84947
Figure 2a, S_0	G.S.	0.91	4.6	0.90	−0.42339	−0.86009
Figure 2c, S_0	G.S.	0.91	11.4	0.90	−0.38041	−0.84922
Figure 1g, S_1	$np_N \rightarrow \pi_{NO}^*$	0.91	72.5	0.89	−0.26850	−0.75189
Figure 1i, S_1	$np_N \rightarrow \pi_{NO}^*$	0.91	82.0	0.89	−0.25178	−0.73668
Figure 2d, S_0	G.S.	0.90	59.2	0.90	−0.30864	−0.77299
Figure 2g, S_0	G.S.	0.87	75.8	0.90	−0.29195	−0.76662
Figure 2f, S_0	G.S.	0.89	63.2	0.90	−0.27592	−0.74659
Figure 2e, S_1	$np_N \rightarrow \pi_{NO}^*$	0.90	115.2	0.89	−0.19594	−0.68382
Figure 1f Ci1[h]		0.85	127.4	0.89	−0.20036	−0.66503
Figure 1e Ci2[h]		0.84	92.7	0.88	−0.20741	−0.67244
D1, S_0	$NH_2(1^2B_1) + NOH^+(1^2A'')$	0.93	125.4	0.89	−0.21296	−0.66756
D2, S_1	$NH_2(1^2B_1) + NOH^+(1^2A')$	0.93	156.8	0.89	−0.15547	−0.61748
D3, S_0	$NH_3(1^1A_1) + NO^+(X1\Sigma^+)$	0.91	34.2[i]	0.87	−0.32246	−0.81420
D4, S_1	$NH_3^+(1^1A_2'') + NO(X^2\Pi)$	0.92	51.3[i]	0.87	−0.31467	−0.78700

[a] Geometries are illustrated in Figures 1 and 2; Ci*n*, denotes conical intersection; D*n*, dissociation products; *n* is an ordinal number. [b] G.S. denotes ground state. [c] Weight of the configuration in the CASPT1 wave function. [d] CASPT2 relative energies in kcal/mol. [e] Weight of the CASSCF reference wave function in the CASPT2 calculation. [f] Absolute CASSCF energy added by 185.0 hartree. [g] Absolute CASPT2 energy added by 185.0 hartree. [h] Values corresponding to the upper solution for the S_1/S_0 conical intersection. [i] These values are referred to the energy of *cis*-NH_3NO^+ in S_0.

cation (NO^+) in the latter, eqs 1 and 2, respectively. The resulting energy curves are displayed in Figure 4.

$$NH_2NOH^+(1^1A') \rightarrow NH_2(1^2B_1) + NOH^+(1^2A') \quad (1)$$

$$NH_3NO^+(1^1A') \rightarrow NH_3(1^1A_1) + NO^+(X^2\Sigma^+) \quad (2)$$

With respect to the former (Figure 4a), its main feature is the occurrence of an S_1/S_0 conical intersection (Ci1, Figure 1f) by means of which the ground state of NH_2NOH^+ correlates with NH_2 (1^2B_1) + NOH^+ ($1^2A''$), the NOH^+ fragment being in its first electronic excited state, while NH_2NOH^+ in its first excited singlet correlates with the fragments in their lowest electronic state, NH_2 (1^2B_1) + NOH^+ ($1^2A'$). Apart from its high energy (∼127 kcal/mol), this dissociation process is hindered by the presence of the conical intersection. Moreover, we have determined by means of MEP calculations (Figure 5a and b) that such a point is connected to the *trans*-NH_2NOH^+ minimum region; consequently, any molecule sampling the surface crossing region would be redirected to this minimum.

With respect to the extrusion of nitrosyl cation (NO^+) (Figure 4b), we have found that the asymptotic limit for the ground state occurs at 34.2 kcal/mol over the *cis*-NH_3NO^+ minimum, and no transition state is present. With respect to the excited states, it is noticed that they are purely dissociative. Additionally, the convergence of the two excited states as the dissociation limit is reached can be observed since the final product corresponds to doubly degenerate ground-state nitric oxide radical.

The dissociation of NH_3NO^+ deserves some more comments. As it is obtained from the linear interpolations, the NH_3^+ fragment can be only generated in the excited state. Considering the fact that at room temperature the nitrosamine−acid complex

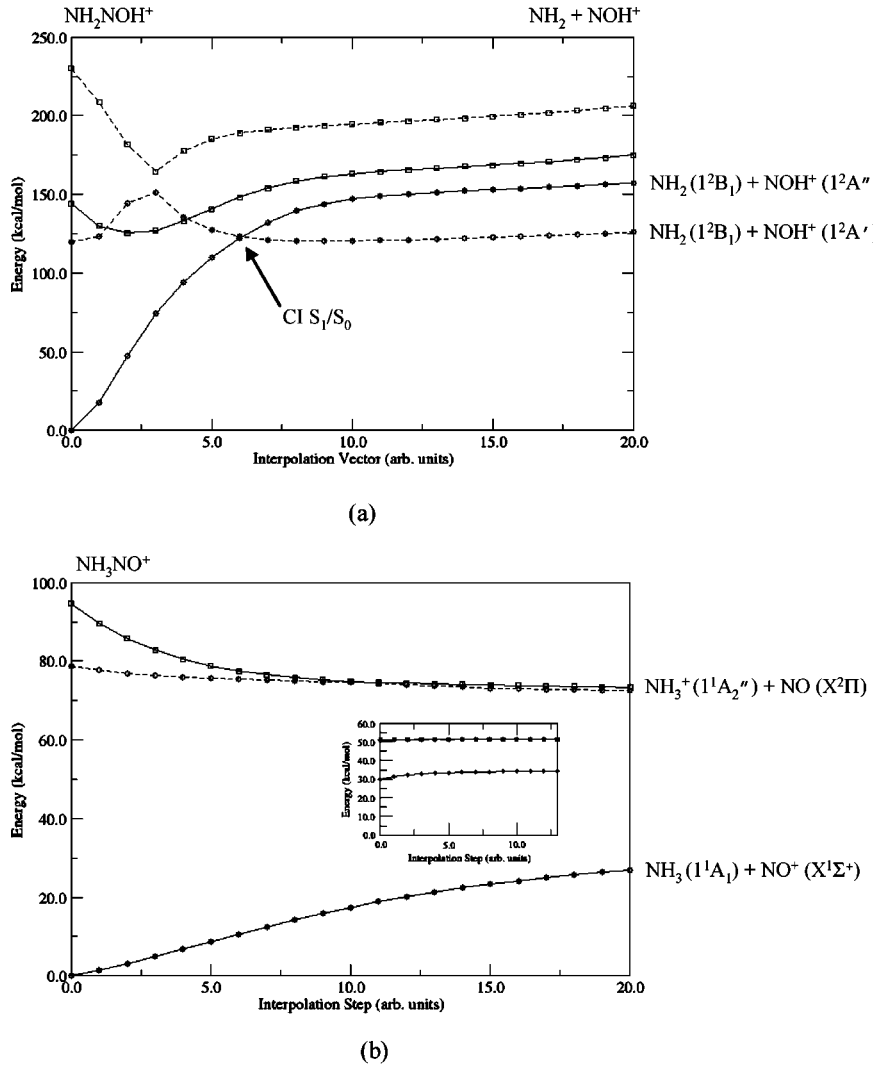

Figure 4. MS-CASPT2 linear interpolations for the N−N homolytic bond scission reactions starting at (a) *trans*-NH_2NOH^+ and (b) *cis*-NH_3NO^+. In the inset in b, the dissociation limits are presented for a final N−N internuclear distance of 30 Å. The dissociation products and their electronic states are represented at the end of each interpolation. The zero-order wave function is SA-CASSCF including two states with equal weights.

dissociates into amminium radical and nitric oxide (see Scheme 1) and that, as shown, protonation occurs after excitation, it can be concluded that the protonation must take place on the excited surface.

C. Vertical Transitions. For the initial study of the upper singlet manifold, MS-CASPT2 vertical transition calculations have been performed at the ground-state relevant geometries, namely, (1) *trans*-NH_2NOH^+, (2) *cis*-NH_2NOH^+, (3) *cis*-NH_3NO^+, and (4) NH_2NHO^+. Table 3 collects the obtained data.

Experimentally, the low-temperature absorption spectrum of nitrosamine−acid complex in a solid matrix exhibits bands at 3.39 eV (367 nm), 3.63 eV (342 nm), and 3.74 eV (333 nm). Moreover, the absorption spectrum of *N*-nitrosodimethylamine in solution has been shown to consist of a low-intensity band at 3.63 eV (342 nm) and a strong band around 5.30 eV (234 nm).[18] By comparing the previous experimental data with the computed MS-CASPT2 vertical transition values for the [NH_2NO-H^+] system (Table 3), it is clear that none of the *trans*-NH_2NOH^+, *cis*-NH_2NOH^+, or NH_2NHO^+ account for the observed lower absorption band and, thus, can be discarded as the responsible species for such absorption. On the other hand, *cis*-NH_3NO^+ can also be ruled out for being the absorbing species despite its similar vertical transition values. Several facts support this assumption. According to experiment,[18] the low-temperature excitation of the nitrosamine−acid complex leads to the formation of a geometry with a tetrahedral amine conformation. This new species absorbs at 3.19, 3.32, and 3.44 eV (391, 375, and 362 nm) and reverses, upon warming, to the initial O-associated complex. These two features are in agreement with both the geometrical features and the MS-CASPT2 vertical transition values of *cis*-NH_3NO^+ (3.46 eV) and with the fact that it is adiabatically connected to *trans*-NH_2NOH^+ as demonstrated by means of the MEP calculations displayed in Figure 3c. Moreover, both the nitrosamine−acid complex and the *N*-nitrosodimethylamine in methylcyclohexane (absence of protons) present very close absorption bands[18] which compare nicely with our previous calculations on neutral nitrosamine (gas phase) [2.98 eV ($f = 0.190 \cdot 10^{-2}$)][7] or neutral NDMA (gas phase and water) [3.29 eV ($f = 0.321 \cdot 10^{-2}$)] and [3.34 eV ($f = 0.327 \cdot 10^{-2}$)], respectively.[8] Therefore, it can be concluded that in the presence of a dilute acid, the absorption bands of *N*-nitrosodimethylamine do not correspond to any protonated species but to the nitrosamine−acid complex, confirming that the proton transfer must take place after excitation.

Furthermore, considering the experimental fact that in diluted acid solution the complex rapidly undergoes photolysis into

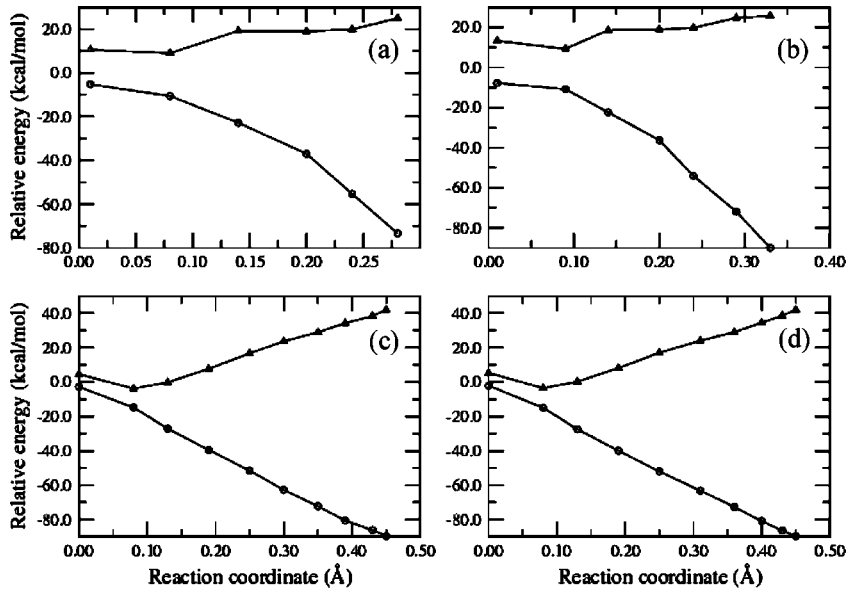

Figure 5. SA-CASSCF minimum energy paths starting at (a) Ci1 following the GD vector direction; (b) Ci1 following the NAC vector direction; (c) Ci2 following the GD vector direction; and (d) Ci2 following the NAC vector direction. In all cases, the initial geometry has been obtained by distorting the reference structure (conical intersection) along the GD or NAC vectors, respectively. SA-CASSCF including two roots with equal weights.

TABLE 3: Vertical Transition Energies (MS-CASPT2) for the Lowest Singlet States of the Relevant Conformers of Protonated Nitrosamine[g]

state[a]	geometry[b]	configuration[c]	weight[d]	ΔE[e]	f[f]
$S_0(1^1A')$	**I**	G.S.	0.91	0.00	
	II	G.S.	0.91	0.48	
	III	G.S.	0.91	0.13	
	IV	G.S.	0.90	0.38	
$S_1(1^1A'')$	**I**	$\sigma_{NO} \rightarrow \pi_{NO}^*$	0.93	5.21	$0.836 \cdot 10^{-2}$
	II	$\sigma_{NN} \rightarrow \pi_{NO}^*$	0.94	6.06	$0.179 \cdot 10^{-1}$
	III	$n\sigma_N \rightarrow \pi_{NO}^*$	0.91	3.46	$0.969 \cdot 10^{-4}$
	IV	$np_O \rightarrow \pi_{NO}^*$	0.94	4.32	$0.205 \cdot 10^{-3}$
$S_2(2^1A')$	**I**	$np_N \rightarrow \pi_{NO}^*$	0.80	6.25	0.218
	II	$np_N \rightarrow \pi_{NO}^*$	0.82	6.84	0.217
	III	$n\sigma_N \rightarrow \pi_{NO}^*$	0.80	4.16	0.269
	IV	$np_N \rightarrow \pi_{NO}^*$	0.76	6.30	0.215

[a] State labeling in C_s notation. All geometries are optimized at the CASSCF level. [b] Conformations according to Scheme 2: **I**, *trans*-NH_2NOH^+ (Scheme 2a); **II**, *cis*-NH_2NOH^+ (Scheme 2b); **III**, *cis*-NH_3NO^+ (Scheme 2c); **IV**, NH_2NHO^+ (Scheme 2d). [c] Character of the electronic transition. [d] Weight of the configuration in the CASPT1 wave function. All calculations are averaged to three states of the same symmetry. [e] Relative energies in eV with respect to ground-state minimum (*trans*-NH_2NOH^+) energy −185.86694 hartree. Applied level shift 0.2. [f] Oscillator strengths in atomic units. [g] SA-CASSCF zero-order wavefunction includes three states with equal weights.

aminium radical[18] and that the nitrosamine acid binding takes place through the oxygen atom,[17] a rearrangement of the complex is expected to take place such that the hydrogen attaches to the amino group nitrogen atom.

D. Nonradiative Deactivation and Nitric Oxide Photorelease. Our starting point for the discussion on the reactivity on S_1 will be the *trans*-NH_2NOH^+ isomer geometry since it is the global minimum of protonated nitrosamine.

At this geometry, the S_1 Franck−Condon point possesses three imaginary frequencies. The most likely pathway, that of the highest frequency in absolute value,[27] leads to a region where degeneracy occurs, a staggered S_1/S_0 conical intersection (Ci2, Figure 1e), as shown by linear interpolations in internal

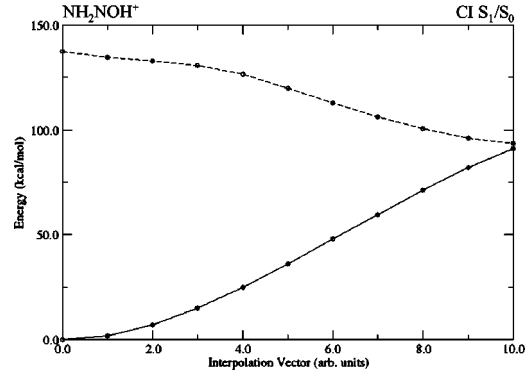

Figure 6. SA-CASSCF (two states with equal weights) energy profiles corresponding to the linear interpolation between NH_2NOH^+ and the S_1/S_0 conical intersection.

coordinates between the Franck−Condon point and the staggered S_1/S_0 conical intersection (Figure 6).

With respect to the possibility of a CASPT2 crossing, if occurring, it is likely to appear in the vicinity of the CASSCF geometry. A nice example of this fact is illustrated in the nitro−nitrite isomerization of nitramide.[30] To investigate the occurrence of such a conical intersection, we have made use of scaled linear interpolations in internal coordinates provided that a standard procedure for the location of a CASPT2 conical intersection is not yet implemented in MOLCAS. In this approach, the interpolation vector between the CASSCF geometries of interest is scaled by a factor (f), and the resulting energy profiles are computed (Figure 7). To survey the minimum energy difference point in the interpolation vector direction, which in turn constitutes our best guess, we have computed a set of MS-CASPT2 linear interpolations built from the same interpolation vector and differing in the scaling factor. As it can be observed, the lowest MS-CASPT2 energy difference between both states is obtained for $f = 1.20$. The location of the energetically closest region between both surfaces cannot be determined a priori and, thus, it is convenient to calculate the whole interpolation.

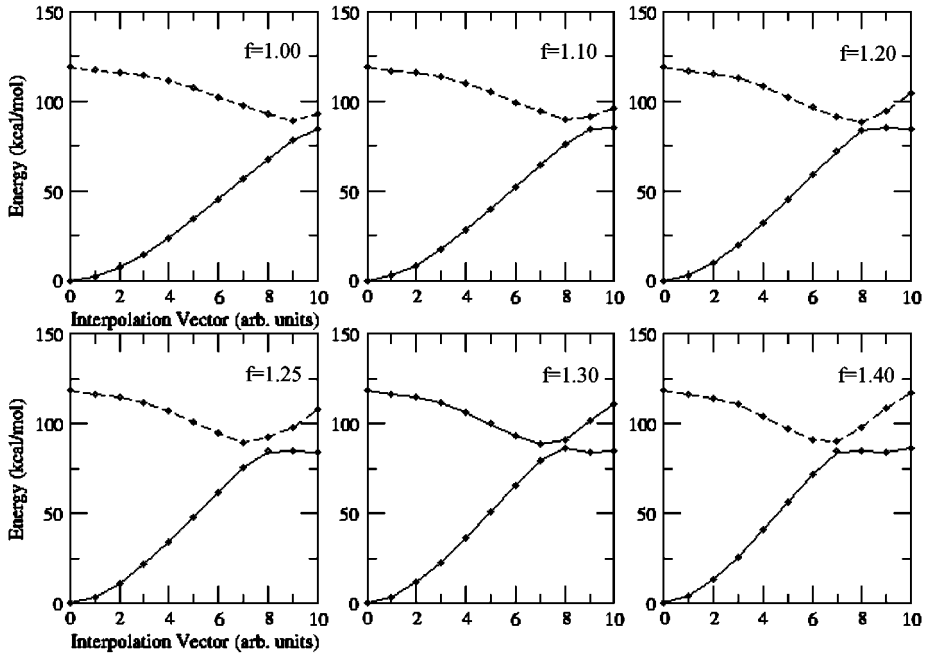

Figure 7. MS-CASPT2 energy profiles corresponding to the scaled linear interpolations between the Franck−Condon geometry and the SA-CASSCF S_1/S_0 conical intersection geometry. In each plot, the interpolation vector is multiplied by the corresponding scaling factor (*f*). The lowest MS-CASPT2 energy difference (~4 kcal/mol) is obtained for $f = 1.20$. SA-CASSCF zero-order wave function includes two states with equal weights.

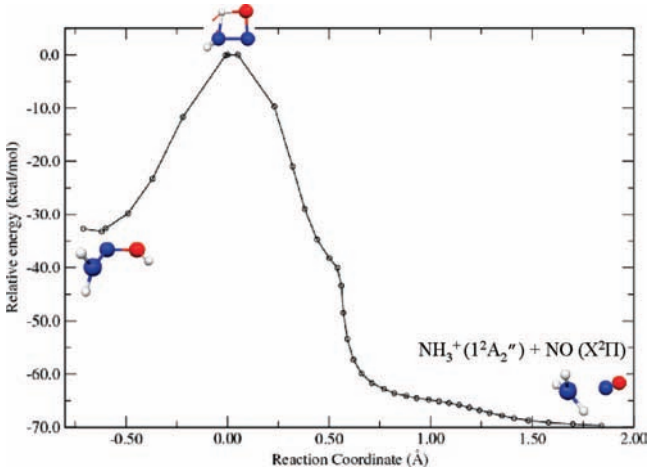

Figure 8. First excited singlet state CASPT2 energy profile (C_s) corresponding to the CASSCF minimum energy path between *cis*-NH_2NOH^+ and the dissociation products $NH_3^+(1^2A_2'') + NO(X^2\Pi)$.

In the region of this conical intersection, a staggered minimum coexists (*stag*-NH_2NOH^+, Figure 1g); however, because of the efficiency of the nonadiabatic process, it is not likely that it results in being populated.

After the surface hop, the degeneracy is lifted (up to first order) along the directions which define the branching space, that is, the gradient difference and the nonadiabatic coupling vectors. If the surface hop occurs exactly at the tip of the cone, the resulting momentum will be oriented along the direction of the gradient difference vector. On the other hand, if the molecule deactivates in the vicinity of the tip, the resulting momentum will be a combination of the initial momentum in the upper surface with the direction defined by the nonadiabatic coupling vector.[27] According to this principle, MEP calculations have been performed along the directions pointed by the gradient difference and the nonadiabatic coupling vectors (Figure 5c and d). As a result, it is obtained that the conical intersection is connected to the *trans*-NH_2NOH^+ minimum region. Hence, after the radiationless deactivation, the molecule reverses to the initial geometry yielding no global reaction and therefore accounting for the photochemical inertia exhibited by O-protonated nitrosamine.

With respect to the photochemistry of NH_3NO^+, this region does not present any minima in S_1. Moreover, it corresponds to a purely dissociative surface in the N−N stretching coordinate as revealed by the energy profiles in Figure 4b. In fact, the only stationary point corresponds to a transition state (Figure 2e) connecting *cis*-NH_2NOH^+ (S_1) (Figure 1i) to its adiabatic decomposition products (eq 3), that is, aminium cation in its ground-state NH_3^+ ($1^2A_2''$) and nitric oxide in its doubly degenerated ground-state NO ($X^2\Pi$). The energy barrier of the transition state with respect to *cis*-NH_2NOH^+ (S_1) is ~33 kcal/mol. A SA-CASSCF MEP calculation along the imaginary mode of this first-order saddle point certainly proves that this is the transition state for eq 3. In Figure 8, we present the CASPT2 energy profile corresponding to the optimal points along the reaction path.

$$NH_3NO^+(S_1) \rightarrow NH_3^+(1^2A_2'') + NO(X^2\Pi) \qquad (3)$$

This previously unreported photochemical channel constitutes evidence of the possibility of nitric oxide photorelease in aliphatic nitrosamines.

To summarize, the major tautomers of protonated nitrosamine exhibit a well-differentiated chemistry. When protonation takes place in the nitroso oxygen atom, a photostable species is formed. On the other hand, if protonation occurs on the amino nitrogen, the resulting molecule presents a purely dissociative excited state which leads to the formation of nitric oxide. The proposed mechanisms would correspond to nitrosamine solutions with large acid concentrations. Nevertheless, from the present results, we have concluded that in the case of low acid concentrations, where a nitrosamine−acid complex is formed, the protonation process must take place after excitation together

with a rearrangement between the O-protonated form and the amino N-protonated form occurring after the nitrosamine−acid complex excitation.

Conclusions

The chemistry of the two lowest singlet states of protonated nitrosamine has been studied. In particular, we have focused on the two most relevant tautomers, namely, *trans*-NH_2NOH^+ and *cis*-NH_3NO^+. The CASPT2//CASSCF methodology has been used throughout this work in conjunction with the ANO-L basis sets. The main results can be summarized as follows.

(1) The mechanism through which aliphatic nitrosamines may act as NO donors has been investigated. The obtained results indicate the involvement of the excited state of the acid-associated nitrosamine which leads to the pyramidalized geometry, *cis*-NH_3NO^+; (2) the proton-transfer reaction between the nitrosamine and the acid takes place in the excited singlet state; (3) an S_1/S_0 conical intersection is responsible for the photostability of NH_2NOH^+; (4) the chemistry of NH_3NO^+ is twofold: while its decomposition on the ground state yields nitrosyl cation (NO^+), excitation to S_1 implies a straightforward release of nitric oxide.

Acknowledgment. This research has been supported by the Spanish Ministerio de Educación y Ciencia (Project BQU2003-1426). Daniel Peláez thanks the Spanish Ministerio de Educación y Ciencia for the Grant BES-2004-6033. Francisco J. Ávila thanks Junta de Andalucía for the Grant P06-FQM-01895.

References and Notes

(1) Magee, P. N.; Barnes, J. M. *Br. J. Cancer* **1956**, *10*, 114–122.
(2) *Concise International Chemical Assessment*; Document No. 38; World Health Organization: Geneva, 2002.
(3) (a) Masuda, S.; Uchida, S.; Terashima, Y.; Kuramoto, H.; Serizawa, M.; Deguchi, Y.; Yanai, K.; Sugiyama, C.; Oguni, I.; Kinae, N. *J. Health Sci.* **2006**, *52*, 211–220. (b) Okafor, P. N.; Nwogbo, E. *Afr. J. Biotechnol.* **2005**, *4*, 1105–1108.
(4) Larsson, S. C.; Bergkvist, L.; Wolk, A. *Int. J. Cancer* **2006**, *119*, 915–919.
(5) (a) Lee, C.; Choi, W.; Kim, Y. G.; Yoon, J. *Environ. Sci. Technol.* **2005**, *39*, 2101–2106. (b) Schreiber, I. M.; Mitch, W. A. *Environ. Sci. Technol.* **2006**, *40*, 6007–6014.
(6) (a) Najmp, I.; Trussel, R. R. *J. AWWA* **2001**, *93*, 92–99. (b) Sen, N. P.; Seaman, S. W.; Brousseau, R. *J. Agric. Food Chem.* **1996**, *44*, 1498–1501.
(7) Peláez, D.; Arenas, J. F.; Otero, J. C.; Soto, J. *J. Chem. Phys.* **2006**, *125*, 164311-11. Additionally selected and published in the November **2006** issue of the *Virtual Journal of Ultrafast Science*.
(8) Peláez, D.; Arenas, J. F.; Otero, J. C.; Soto, J. *J. Org. Chem.* **2007**, *72*, 4741–4749.
(9) Geiger, G.; Huber, J. R. *Helv. Chim. Acta* **1981**, *64*, 989–995.
(10) (a) Persico, M.; Cacelli, I.; Ferretti, A. *J. Chem. Phys.* **1991**, *94*, 5508–5523. (b) Cimaraglia, R.; Persico, M.; Tomasi, J. *J. Am. Chem. Soc.* **1985**, *107*, 1617–1622.
(11) Chow, Y. L. *Acc. Chem. Res.* **1973**, *6*, 354–360.
(12) Cessna, A. J.; Sugamori, S. E.; Yip, R. W.; Lau, M. P.; Zinder, R. S.; Chow, Y. L. *J. Am. Chem. Soc.* **1977**, *99*, 4044–4048.
(13) Yip, R. W.; Vidoczy, T. W.; Snyder, R.; Chow, Y. L. *J. Phys. Chem.* **1978**, *82*, 1194–1200.
(14) Forzatti, P.; Nova, I.; Castoldi, L. *Chem. Biochem. Eng. Q.* **2005**, *19*, 309–323.
(15) Egsgaard, H.; Carlsen, L.; Madsen, J. Ø. *Chem. Phys. Lett.* **1994**, *227*, 33–38.
(16) Kulkarni, S. A.; Pundlik, S. S. *Chem. Phys. Lett.* **1995**, *245*, 143–149.
(17) Layne, W. S.; Jaffé, H. H.; Zimmer, H. J. *J. Am. Chem. Soc.* **1967**, *85*, 435–438.
(18) Chow, Y. L.; Wu, Z.-Z.; Law, M.-P.; Yip, R. W. *J. Am. Chem. Soc.* **1985**, *107*, 8196–8201.
(19) (a) Yanagimoto, T.; Toyota, T.; Matsuki, N.; Makino, Y.; Uchiyama, S.; Ohwada, T. *J. Am. Chem. Soc.* **2007**, *129*, 736–737. (b) Pavlos, C. M.; Cohen, A. D.; D'Sa, R. A.; Sunoj, R. B.; Wasylenko, W. A.; Kapur, P.; Relyea, H. A.; Kumar, N. A.; Hadad, C. M.; Toscazo, J. P. *J. Am. Chem. Soc.* **2003**, *125*, 14934–14940.
(20) Ohwada, T.; Miura, M.; Tanaka, H.; Sakamoto, S.; Yamaguchi, K.; Ikeda, H.; Inagaki, S. *J. Am. Chem. Soc.* **2001**, *123*, 10164–10172.
(21) Wang, X.; Tanus-Santos, J. E.; Reiter, C. D.; Dejam, A.; Shiva, S.; Smith, R. D.; How, N.; Gladwin, M. T. *Proc. Natl. Acad. Sci. U.S.A.* **2004**, *101*, 11477–11482.
(22) (a) Andersson, K.; Malmqvist, P.-Å.; Roos, B. O.; Sadlej, A. J.; Wollinski, K. *J. Phys. Chem.* **1990**, *94*, 5483–5488. (b) Andersson, K.; Malmqvist, P.-Å.; Roos, B. O. *J. Chem. Phys.* **1992**, *96*, 1218–1226. (c) Finley, J.; Malmqvist, P.-Å.; Roos, B. O.; Serrano-Andrés, L. *Chem. Phys. Lett.* **1998**, *288*, 299–306.
(23) Roos, B. O. In *Advances in Chemical Physics*; Lawley, K. P., Eds.; Ab Initio Methods in Quantum Chemistry; Wiley: Chichester, U.K., 1987; Chapter 69, *Vol. 2*, p 399.
(24) Widmark, P.-O.; Malmqvist, P.-Å.; Roos, B. O. *Theor. Chim. Acta* **1990**, *77*, 291–306.
(25) Veryazov, V.; Widmark, P.-O.; Serrano-Andrés, L.; Lindh, R.; Roos, B. O. *Int. J. Quantum Chem.* **2004**, *100*, 626–635.
(26) Frisch, M. J.; Trucks, G. W.; Schlegel, H. B.; Scuseria, G. E.; Robb, M. A.; Cheeseman, J. R.; Montgomery, J. A., Jr.; Vreven, T.; Kudin, K. N.; Burant, J. C.; Millam, J. M.; Iyengar, S. S.; Tomasi, J.; Barone, V.; Mennucci, B.; Cossi, M.; Scalmani, G.; Rega, N.; Petersson, G. A.; Nakatsuji, H.; Hada, M.; Ehara, M.; Toyota, K.; Fukuda, R.; Hasegawa, J.; Ishida, M.; Nakajima, T.; Honda, Y.; Kitao, O.; Nakai, H.; Klene, M.; Li, X.; Knox, J. E.; Hratchian, H. P.; Cross, J. B.; Bakken, V.; Adamo, C.; Jaramillo, J.; Gomperts, R.; Stratmann, R. E.; Yazyev, O.; Austin, A. J.; Cammi, R.; Pomelli, C.; Ochterski, J. W.; Ayala, P. Y.; Morokuma, K.; Voth, G. A.; Salvador, P.; Dannenberg, J. J.; Zakrzewski, V. G.; Dapprich, S.; Daniels, A. D.; Strain, M. C.; Farkas, O.; Malick, D. K.; Rabuck, A. D.; Raghavachari, K.; Foresman, J. B.; Ortiz, J. V.; Cui, Q.; Baboul, A. G.; Clifford, S.; Cioslowski, J.; Stefanov, B. B.; Liu, G.; Liashenko, A.; Piskorz, P.; Komaromi, I.; Martin, R. L.; Fox, D. J.; Keith, T.; Al-Laham, M. A.; Peng, C. Y.; Nanayakkara, A.; Challacombe, M.; Gill, P. M. W.; Johnson, B.; Chen, W.; Wong, M. W.; Gonzalez, C.; Pople, J. A. Gaussian 03, revision C.02; Gaussian, Inc.: Wallingford, CT, 2004.
(27) (a) Blais, N. C.; Truhlar, D. G.; Mead, C. A. *J. Chem. Phys.* **1988**, *89*, 6204–6208. (b) Stine, J. R.; Muckerman, J. C. *J. Phys. Chem.* **1987**, *91*, 459–466. (c) Arenas, J. F.; Otero, J. C.; Peláez, D.; Soto, J. *J. Chem. Phys.* **2005**, *122*, 084324-11. (d) Arenas, J. F.; Otero, J. C.; Peláez, D.; Soto, J. *J. Phys. Chem. A* **2005**, *109*, 7172–7180. (e) Arenas, J. F.; López-Tocón, I.; Otero, J. C.; Soto, J. *J. Am. Chem. Soc.* **2002**, *124*, 1728–1735.
(28) (a) Arenas, J. F.; Otero, J. C.; Peláez, D.; Soto, J. *J. Chem. Phys.* **2003**, *119*, 7814–7823. (b) Arenas, J. F.; Centeno, S. P.; López-Tocón, I.; Peláez, D.; Soto, J. *J. Mol. Struct.: THEOCHEM* **2003**, *630*, 17–23.
(29) Arenas, J. F.; Otero, J. C.; Peláez, D.; Soto, J. *J. Org. Chem.* **2006**, *71*, 983–991.
(30) Soto, J.; Arenas, J. F.; Otero, J. C.; Peláez, D. *J. Phys. Chem. A* **2006**, *110*, 8221–8226.
(31) Merchán, M.; González-Luque, R.; Climent, T.; Serrano-Andrés, L.; Rodríguez, E.; Reguero, M.; Peláez, D. *J. Phys. Chem. B* **2006**, *110*, 26471–26476.
(32) Arenas, J. F.; Ávila, F. J.; Otero, J. C.; Peláez, D.; Soto, J. *J. Phys. Chem. A* **2008**, *112*, 249–255.
(33) Bode, B. M.; Gordon, M. S. *J. Mol. Graphics Modell.* **1999**, *16*, 133.
(34) (a) Arenas, J. F.; Otero, J. C.; Peláez, D.; Soto, J.; Serrano-Andrés, L. *J. Chem. Phys.* **2004**, *121*, 4127–4132. (b) Arenas, J. F.; Marcos, J. I.; López-Tocón, I.; Otero, J. C.; Soto, J. *J. Chem. Phys.* **2000**, *113*, 2282–2289.
(35) Forsberg, N.; Malmqvist, P.-Å. *Chem. Phys. Lett.* **1997**, *274*, 196–204.
(36) Malmqvist, P.-Å. *Int. J. Quantum Chem.* **1986**, *30*, 479–494.
(37) Aschi, M.; Grandinetti, F. *Chem. Phys. Lett.* **1997**, *267*, 98–104.
(38) Gerbaux, P.; Wantier, P.; Flammang, R. *J. Am. Soc. Mass Spectrom.* **2004**, *15*, 344–355.

JP803252H